Int. J. Electrochem. Sci., 17 **(2022)** Article Number: 22035, doi: 10.20964/2022.03.06

International Journal of
ELECTROCHEMICAL
SCIENCE
www.electrochemsci.org

Understanding of the Corrosion Behavior of Carbon Steel in the NH_4Cl-H_2S-CO_2 Coexisting Environment

Haibo Wang[1,*], *Chi Zhang*[1], *Changsui Lu*[2,*], *Hongyuan Wang*[3], *Xingguang Shi*[3], *Huiyu Shi*[1], *Weiming Lu*[1]

[1] College of Environmental and Safety Engineering, Shenyang University of Chemical Technology, Shenyang 110142, PR China
[2] China Construction Industrial &Energy Engineering Group Co., LTD, Nanjing 210046, PR China
[3] Ningbo special equipment inspection institute, Ningbo 315048, PR-China
[*]E-mail: wanghaibo@syuct.edu.cn; 421170894@qq.com

Received: 23 October 2021 / *Accepted:* 24 December 2021 / *Published:* 2 February 2022

In this work, NH_4Cl corrosion induced failure accompanied by H_2S and CO_2 corrosion in the overhead systems of a hydrotreater was studied. Electrochemical impedance spectroscopy (EIS) and potentiodynamic polarization techniques were used to evaluate the effect of temperature, low-level H_2S and pH on the corrosion behavior of carbon steel in NH_4Cl-H_2S-CO_2 coexisting environment. The results indicated the presence of H_2S (10 ppm) that inhibited the corrosion of the carbon steel in the H_2S-CO_2-NH_4Cl corrosion system at 60 ℃. In this case, the minimum corrosion rate of 0.7 mm/y could be achieved. H_2S played a key role in influencing the cathodic and anodic reactions. The corrosion rate increased rapidly with the increase in H_2S concentration above >10 ppm, and the relationship between the corrosion rate and the concentration of H_2S was established. The dominant cathodic reaction was found to be the carbonic acid reduction at pH > 4, meaning that H_2S-CO_2-NH_4Cl induced corrosion can be effectively controlled by adjusting the content of H_2S component.

Keywords: H_2S corrosion; NH_4Cl corrosion; CO_2 corrosion; Corrosion behavior.

1. INTRODUCTION

In the last years, more and more refineries have exhibited the NH_4Cl corrosion problems under harsh environments associated with poor quality of the crude oil [1, 2]. In particular, NH_4Cl comes from NH_3 and HCl as a result of the decomposition and cracking of the crude oil in the reactive tower. Moreover, the corrosive media in the oil refinery industry usually contain relevant amounts of CO_2 and H_2S that induce local corrosion, pitting corrosion, cracking and failure of related industrial facilities, which may cause a significant threat to employee safety as well as a serious environmental concern. Meanwhile, the H_2S corrosion mechanism remains still poorly understood when compared to that

induced by CO_2. This is because H_2S is a toxic flammable gas and the relevant reactions are hard to control. Today, the severity of H_2S corrosion is one of the most pressing matters in oil refineries, requiring a thorough study in this field of industry [3].

A simultaneous presence of CO_2 and H_2S compounds promotes corrosion of steel, which may lead to the formation of FeS and $FeCO_3$ films [4] on the surface of steel, making it difficult to accurately quantify the corrosion rate. In that regard, special attention has been paid to the corrosion behavior in the mixed H_2S and CO_2 environments [5-7]. For instance, Dong et al. [8] studied the corrosion of AFLAS, FKM and HNBR rubber materials in the packer, exhibiting the emergence of CO_2 and H_2S and the results indicated that HNBR rubber had the worst corrosion resistance capability. Moreover, Li et al. [9] monitored the evolution of corrosion of austenitic stainless steel in $H_2S/CO_2/Cl^-$ coexisting environment, finding that the corrosion resistance of the steels can be improved by coating them with an S-phase layer. Besides, the morphology of iron sulfide films formed in H_2S and CO_2 environments was studied by Svenningsen et al. [10] who showed that the film growth rates were limited by the electronic conductivity. In addition, the inhibitive effect of 10 ppm H_2S on the NH_4Cl induced corrosion of carbon steel was carefully investigated in Ref. [11]. It is noteworthy that, in the processing units of typical petroleum refineries such as hydrotreaters, the corrosion caused by NH_4Cl salt deposition is accompanied by the corrosion in CO_2 and H_2S acid gas media [12, 13] which would result in catastrophic accidents and huge economic losses. Therefore, understanding and controlling NH_4Cl-H_2S-CO_2 induced corrosion is one of the urgent tasks for the refinery industry.

The development of effective methods of preventing accidental failure of facilities is a major challenge, especially because of the lack of information on the corrosion mechanisms in the H_2S-CO_2-NH_4Cl coexisting environment. Thus, the present study is aimed at investigating the influence of H_2S on the corrosion behavior of carbon steel in the CO_2-NH_4Cl coexisting environment to simulate the overhead systems of refinery equipment. Special attention is paid to the effect of H_2S at low (ppm level) concentrations on carbon steel corrosion in the CO_2-NH_4Cl corrosive environment. Besides, the effects of environmental factors on the corrosion behavior of carbon steel are investigated, including the temperature (between 30 and 90 ℃) and acidity (with the pH range from 2 to 6.24).

2. MATERIALS AND METHODS

2.1. Materials and reagents

The material under consideration was AISI 20# carbon steel including 0.38% Si, 0.21% C, 0.09% P, 0.05% S, 0.05% Mn and balance Fe (wt.%). Copper wires were afterwards welded to the back of the steel specimens and filled with epoxy resin to make the working electrodes (WE). The surface of each WE was polished with 2000 mesh wet sandpaper and Al_2O_3 powder (0.001 mm) impregnated with a polishing cloth. Deionized water and alcohol were finally used to clean the WE surfaces.

2.2 Electrochemical measurements

To investigate the corrosion behavior of carbon steel, electrochemical tests were performed on a glass cell with a three-electrode system consisting of a saturated Ag/AgCl electrode, a platinum electrode and a WE. As soon as the measured value of the open circuit potential was stabilized within ±5 mV for at least 30 min, the electrochemical impedance spectroscopy (EIS) (the frequency range from 100 KHz to 10 MHz) or potentiodynamic sweep (a sweep rate of 0.5 mV/s) tests were initiated.

2.3 Experimental procedures

To elucidate the effect of temperature on the corrosion behavior of carbon steel, the specimens were subjected to saturated CO_2 medium with 10 ppm H_2S and 0.5 mol % NH_4Cl solution for 7 h at 30°C, 45°C, 60°C, 75°C, and 90°C, respectively

The same corrosive conditions were used to investigate the influence of H_2S concentration on the steel, by varying the amount of H_2S as 5, 10, 20, 40, 80, 160 and 320 ppm and keeping the temperature of environment at 60°C.

The impact of acidity (at pH levels of 2, 3, 4, and 6) of NH_4Cl solution (0.5 mol%) on the corrosion behavior of carbon steel was also examined by leaving specimens in the corrosive medium for 7 h at 60°C.

3. RESULTS AND DISCUSSION

3.1 Effect of temperature on the corrosion behavior of carbon steel

Figure 1 displays the polarization cures of carbon steel after exposure in 0.5 mol% NH_4Cl solution at different reaction temperatures (30, 45, 60, 75, 90°C). In turn, Table 1 shows the corresponding electrochemical parameters. It was evident that the acid gas solubility was higher at the temperatures below 60°C and more H^+ ions were dissociated, the hydrogen reduction was the dominant cathodic reaction at those conditions. In turn, the minimum corrosion rate (CR = 0.07 mm/y) was reached at 60°C, which then increased to 0.86 mm/y at 90°C. Generally, it is believed that there is a directly proportional relationship between CR and temperature. However, if there was the presence of CO_2 in the corrosion process, the law of effects would be more complicated. Since the $FeCO_3$ film formed at 60℃ was more stable than those at the higher or lower temperatures, it restricted the transfer of the corrosive reactants [14].

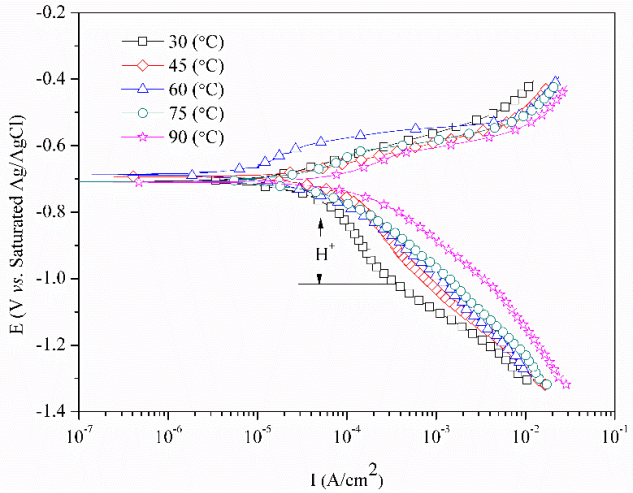

Figure 1 Polarization curves of carbon steel after exposure to 0.5 mol% NH_4Cl solution with saturated CO_2 and 10 ppm H_2S for 7 h at different reaction temperatures.

Table 1. Polarization parameters evaluated from the curves in Figure 1.

Temperature (°C)	B_a (mV/decade)	B_c (mV/decade)	$I_o \times 10^{-5}$ (A/cm^2)	E_o (mV)	CR (mm/y)
30	93	–170	2.00	–708	0.23
45	72	–167	3.70	–693	0.44
60	83	–139	0.56	–688	0.07
75	95	–130	2.18	–708	0.26
90	93	–147	7.28	–710	0.86

To further verify the above conclusion, the Nyquist plots (Fig. 2) were acquired to track the evolution of the impedance signature characteristic of the steel at different temperatures. In all cases, a capacitive loop was observed in the high-frequency region, which corresponded to a charge-transfer resistance.

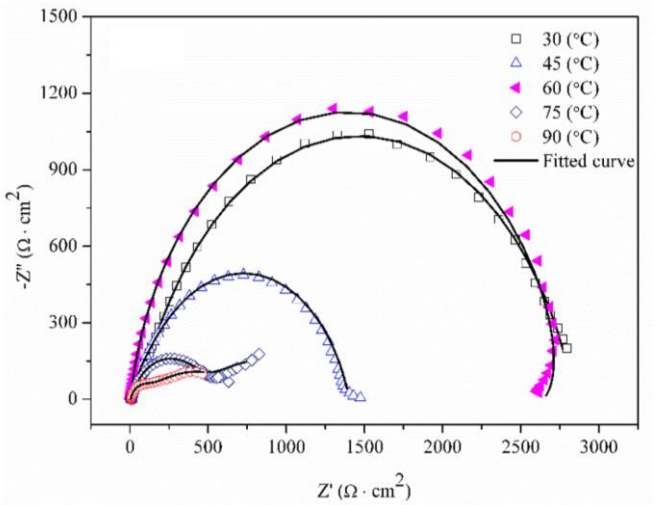

Figure 2. Nyquist plots of carbon steel in NH_4Cl (0.5 mol%) solution with CO_2 (saturated) and H_2S (10 ppm) at a different temperatures.

For the low-frequency region, an inductive loop appeared at 60°C, which was related to the adsorption of an intermediate product on the metal surface. Table 2 shows the impedance parameters obtained after fitting the Nyquist plots using the electrical equivalent circuit given in Fig. 3. The Nyquist plots at 30, 45, 75, and 90°C were fitted by means of the equivalent circuit from Fig. 3(a), while that at 60°C was described with the equivalent circuit from Fig. 3(b). The maximum diameter of the capacitive loop (2660 $\Omega \cdot cm^2$) was found at 60°C that indicated the resulting film possessed the best protective function under the mentioned conditions.

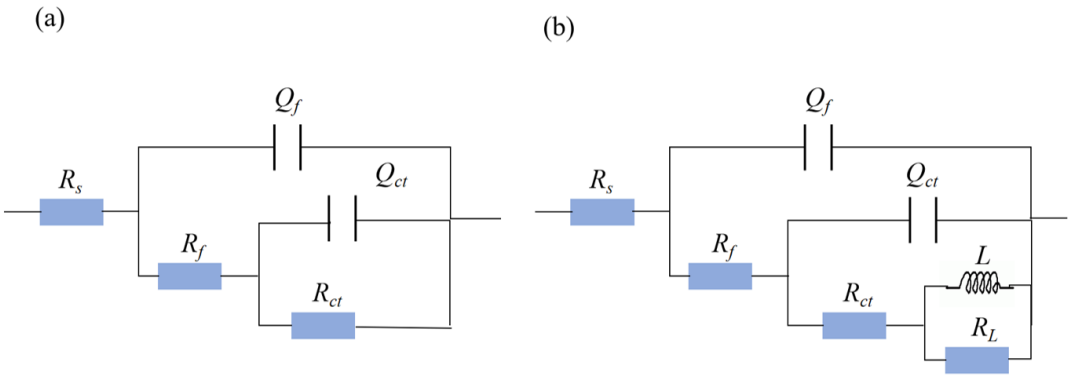

R_s: the solution resistance;
R_f: the resistance of the corrosion products formed on the surface;
R_{ct}: the charge transfer resistance;
Q_f: the constant phase angle elements representing the corrosion product film capacitance (C_f);
Q_{ct}: double-layer capacitance (C_{ct});
R_L: the resistance of relaxation process by adsorbed ions and protons;
L : the inductance of relaxation process by adsorbed ions and protons.

Figure 3. Electrical equivalent circuit.

Table 2 The impedance parameters found from the Nyquist plots (Figure 2).

T(°C)	R_s	Q_f		R_f	Q_{ct}		R_{ct}	R_L	L
	(Ω cm^2)	(Ω^{-1} cm^{-2} S^n)	n_f	(Ω cm^2)	(Ω^{-1} cm^{-2} S^n)	n_{dl}	(Ω cm^2)		
30	9.055	8.741×10^{-5}	0.866	267	1.566×10^{-4}	0.792	2567	-	-
45	7.159	1.318×10^{-4}	0.849	413	1.785×10^{-4}	0.754	981.9	-	-
60	4.797	1.742×10^{-5}	-	4.701	4.778×10^{-5}	0.766	2660	541.7	185.9
75	6.684	1.501×10^{-3}	0.748	442.8	6.557×10^{-3}	0.435	832	-	-
90	5.616	1.232×10^{-4}	0.863	91.01	3.516×10^{-3}	0.382	681.2	-	-

Tables 3 shows the CRs of carbon steel in NH_4Cl-H_2S, NH_4Cl-CO_2, and NH_4Cl-H_2S-CO_2 environments at different temperatures. It is noteworthy that CRs of carbon steel in NH_4Cl (0.5 mol%),

NH_4Cl-H_2S(10 ppm) and NH_4Cl-CO_2 environments were estimated in previous works to be 0.08, 0.07 and 4.23 mm/y at 30°C [11, 24], respectively. In other words, the CR of carbon steel in the NH_4Cl-CO_2 medium was higher than that in the NH_4Cl-H_2S environment at the same temperature. This is due to the fact that CO_2 is the acidic gas which accelerates the corrosion of the carbon steel. In present study, the CR of the carbon steel in the NH_4Cl-H_2S-CO_2 environment was 0.23 mm/y at 30°C, being lower than that under the NH_4Cl-CO_2 conditions. This indicated the CO_2 induced corrosion was the dominant corrosion reaction. At the same time, H_2S exerted the retarding effect on the corrosion rate of the carbon steel. In particular, the lowest corrosion rate was achieved in the NH_4Cl-H_2S-CO_2 (0.07 mm/y) and NH_4Cl-CO_2 (0.73 mm/y) environments at 60°C. This change law of CR from 30°C to 75°C in the NH_4Cl-H_2S-CO_2 medium was consistent with the results obtained in the NH_4Cl-CO_2 environment in Ref. [24]. This could be explained by the easier formation of $FeCO_3$ products with a dense structure adhered on the metal surface at 60°C in CO_2 environment [24].

Table 3. The CRs of carbon steel in NH_4Cl-H_2S, NH_4Cl-CO_2, and NH_4Cl-H_2S-CO_2 environments at different temperatures.

Temperature	CR (mm/y)		
	0.5 mol% NH_4Cl-10 ppmH_2S [11]	0.5 mol% NH_4Cl-saturated CO_2 [24]	0.5 mol% NH_4Cl-10 ppm H_2S-saturated CO_2
30°C	0.07	4.23	0.23
45°C	0.10	1.03	0.44
60°C	0.20	0.73	0.07
75°C	0.75	2.09	0.26

3.2 Effect of pH on the corrosion behavior of carbon steel

The effect of acidity (pH levels of 2, 3, 4, and 6) of NH_4Cl solution (0.5 mol%) on the polarization curves of carbon steel was investigated based on the polarization curves in Fig. 4, and the corresponding electrochemical parameters were listed in Table 4. The variation of the anodic branch polarization curves at different pH was very small, but the cathodic limiting current density increased significantly with the decrease of pH. In particular, the CR value increased from 0.07 mm/y to 2.31 mm/y with decreasing pH from 6.24 to 2. In turn, the limiting current was reduced from 3.35 A/cm^2 at pH of 4 to 2.05 A/cm^2 at pH of 6. However, there was a significant decrease in the current density from 19.66 A/cm^2 at pH of 2 to 3.35 A/cm^2 at pH of 4. These results indicated that the hydrogen reduction was the dominant cathodic reaction at the lower levels of acidity of the corrosive solution (pH of 3 and pH of 2). According to the EIS diagrams in Fig. 5, the diameter of the impedance semicircle increased with increasing pH. Moreover, the high-frequency capacitance semicircle and the low-frequency inductance semicircle were

observed in the electrodes at pH of 6.24. At other pH values, there were the high-frequency and low-frequency capacitance semicircles in the Nyquist diagrams. The corresponding Bode plots revealed that the peak with a maximum phase angle decreased and shifted toward the lower frequencies with an increase in pH, which is usually associated with an increase of double-layer capacitance with rising pH level.

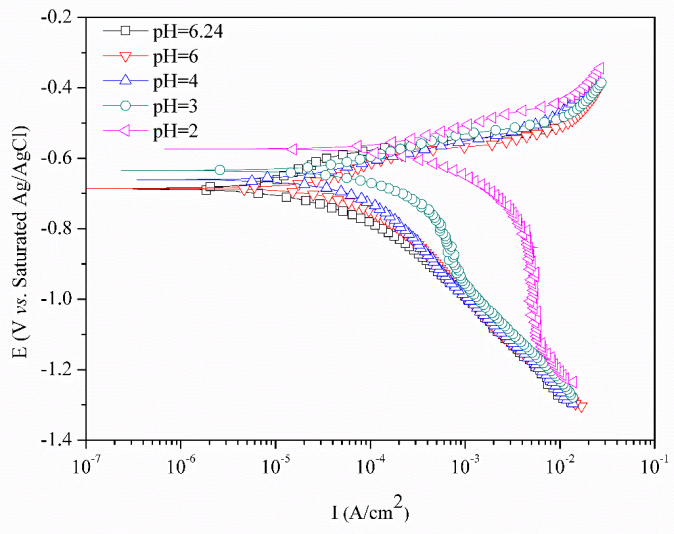

Figure 4. The polarization curve of carbon steel in NH_4Cl (0.5 mol %) solution with CO_2 (saturated) and H_2S (10 ppm) at a different pH for 7 h at 60℃.

Table 4. Potentiodynamic polarization parameters of Fig 4.

pH	B_a (mV/decade)	B_c (mV/decade)	$I_o \times 10^{-5}$ (A/cm^2)	E_o (mV)	CR (mm/y)
2	84	–123	19.66	–573	2.31
3	76	–121	4.41	–635	0.52
4	83	–154	3.35	–661	0.39
6	80	–126	2.05	–685	0.24
6.24	83	–139	0.56	–688	0.07

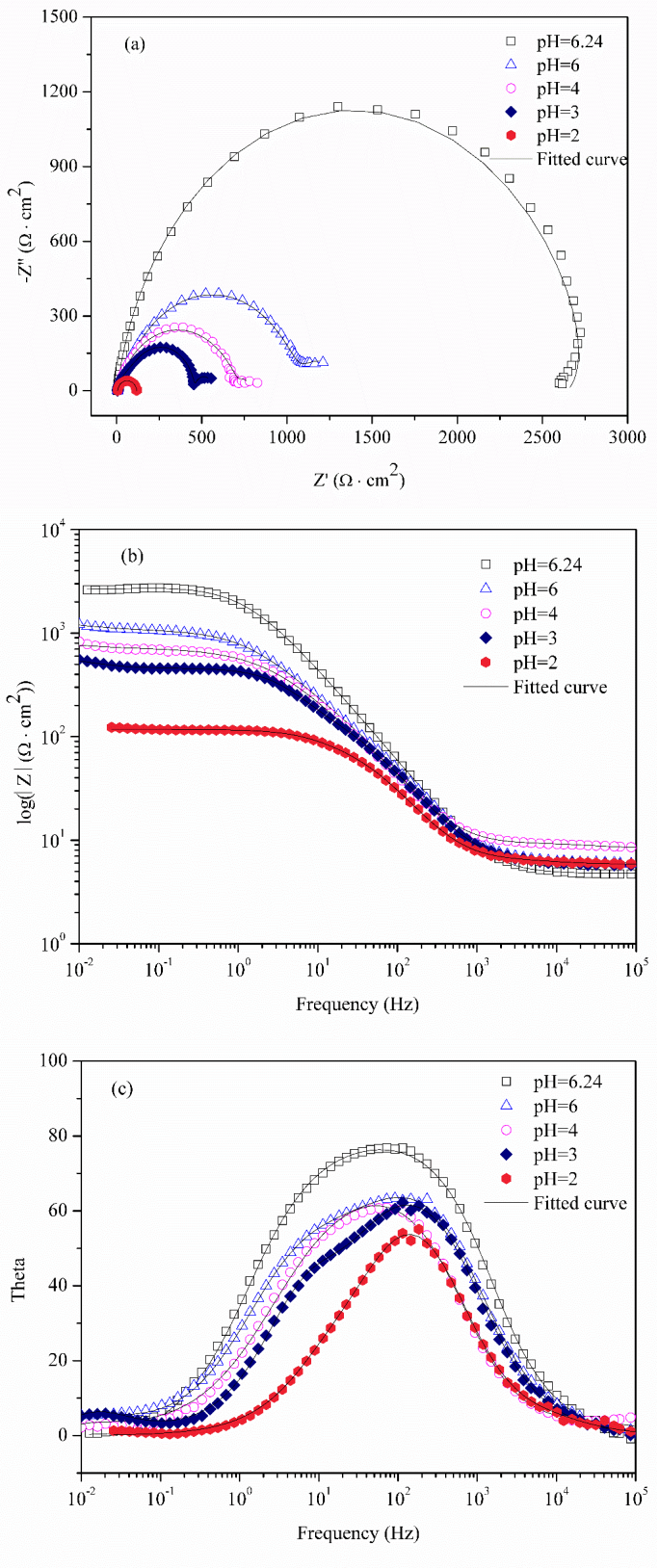

Figure 5. EIS curves of carbon steel in NH_4Cl (0.5 mol %) solution with CO_2 (saturated) and H_2S (10 ppm) at a different pH for 7 h at 60°C.

The CRs of carbon steel in NH_4Cl-H_2S, NH_4Cl-CO_2, and NH_4Cl-H_2S-CO_2 environments at different pH levels are shown in Table 5. The corrosion rate varied as follows: NH_4Cl-10 ppm H_2S < NH_4Cl-10 ppm H_2S-saturated CO_2 < NH_4Cl-saturated CO_2. $FeCO_3$ was unstable at pH < 4 and therefore lost its protection to steel [20, 21]. In turn, the CR values of carbon steel in NH_4Cl-10 ppm H_2S, NH_4Cl-saturated CO_2 and NH_4Cl-10 ppm H_2S-saturated CO_2 media at pH of 6 were 0.17, 0.68 and 0.24 mm/y, respectively. A decrease in corrosion rate was due to the fact that H_2S reacted directly with iron, leading to the formation of a stable mackinawite (FeS) phase on the steel surface at pH > 5 [22, 23]. This phase consequently acted as a diffusion barrier to reduce the corrosion. Besides, the dominant cathodic reaction at a lower pH level (pH < 4) was the hydrogen reduction and that at a higher pH value (pH > 4) was the carbonic acid reduction.

Table 5. The CRs of carbon steel in NH_4Cl-H_2S, NH_4Cl-CO_2, and NH_4Cl-H_2S-CO_2 environments at different pH levels.

pH	Corrosion Rate (mm/y) at 60°C		
	0.5 mol% NH_4Cl-10ppmH_2S [11]	0.5 mol% NH_4Cl-saturated CO_2 [24]	0.5 mol% NH_4Cl-10ppm H_2S-saturated CO_2
2	5.44	6.81	2.31
3	0.66	1.99	0.52
4	0.30	1.09	0.39
6	0.17	0.68	0.24

3.3 Effect of H_2S concentration on the corrosion behavior of carbon steel

Figures 6 and 7 depict the polarization curves and EIS plots of carbon steel in NH_4Cl solution (0.5 mol%) with saturated CO_2 at 60℃ and different H_2S concentrations. The electrochemical parameters extracted from those graphs are given in Tables 6 and 7, respectively. The CR value of carbon steel was 0.13 mm/y for 5 ppm H_2S, and 0.07 mm/y for 10 ppm H_2S. With a further increase in H_2S concentration from 10 ppm to 360 ppm, the corrosion rate increased from 0.07 mm/y to 0.44 mm/y. As seen, the presence of 10 ppm H_2S led to a reduction of corrosion rate to 0.07 mm/y. The equivalent circuit from Fig. 3(b) was used to evaluate the Nyquist plots at 10 ppm H_2S, while Fig. 3(a) was applied for other concentrations. The diameter of the capacitive loop in the system with a 5ppm H_2S concentration was lower than that at 10ppm H_2S. Moreover, the high-frequency capacitive semicircle decreased and the time constant became shorter with an increase in the H_2S concentration from 10 ppm to 320 ppm. The maximum diameter of the capacitive loop was 2660 Ω cm^2 at 10 ppm H_2S with a minimum corrosion rate (0.07 mm/y).

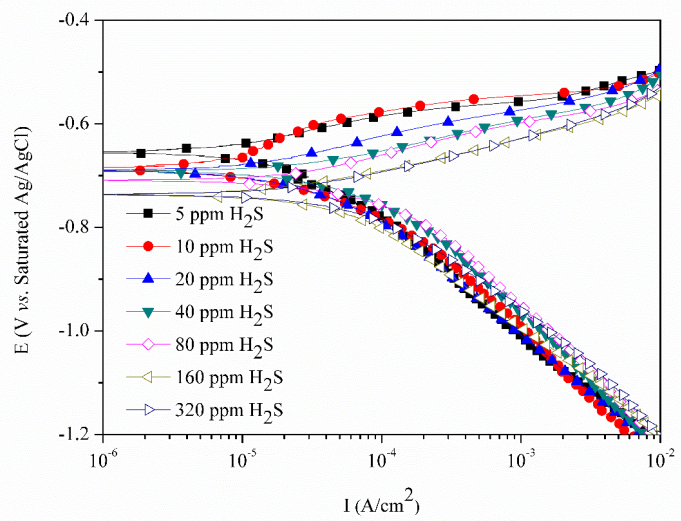

Figure 6. Polarization curves of carbon steel in NH_4Cl (0.5 mol %) solution with CO_2 (saturated) at different H_2S concentrations for 7 h at 60°C.

Table 6. Potentiodynamic polarization parameters extracted from data in Figure 6.

H_2S (ppm)	B_a (mV/decade)	B_c (mV/decade)	$I_o \times 10^{-5}$ (A/cm^2)	E_o (mV)	CR (mm/y)
5	46	–163	1.12	–635	0.13
10	83	–139	0.56	–688	0.07
20	67	–144	1.42	–690	0.17
40	72	–146	2.58	–693	0.30
80	76	–121	3.16	–709	0.37
160	75	–168	3.39	–737	0.40
320	77	–141	3.70	–736	0.44

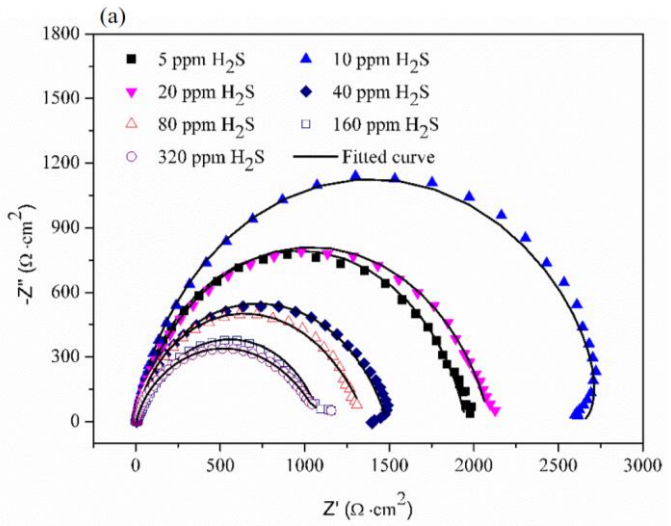

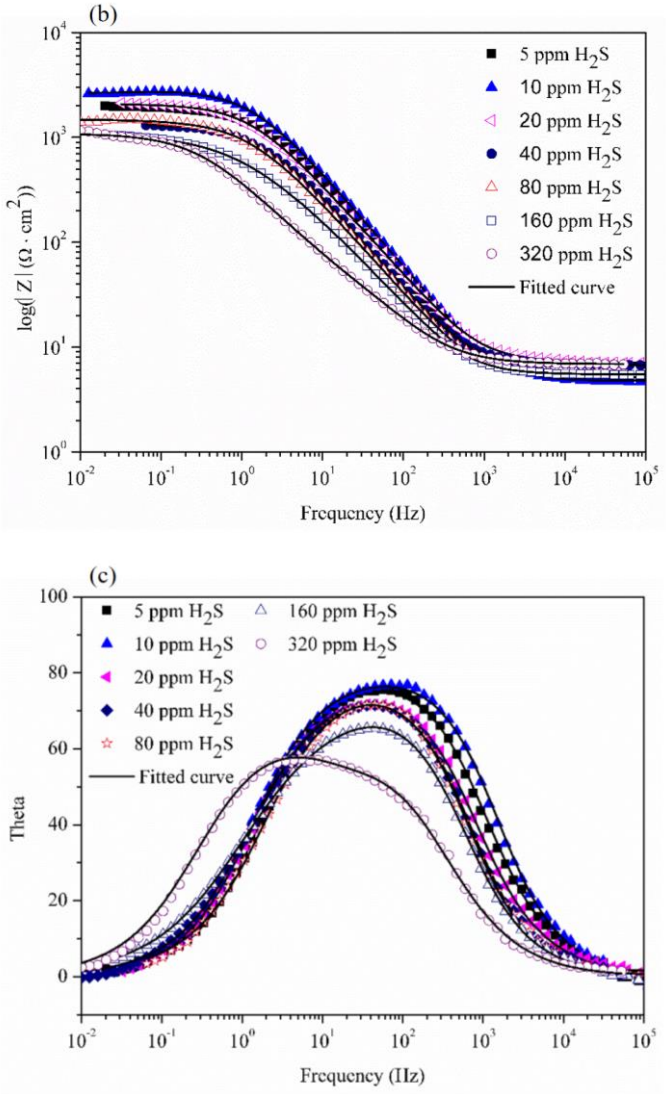

Figure 7. Impedance results obtained at different H_2S concentrations in 0.5 mol% NH_4Cl solution with the CO_2 saturated solution at 60°C: Nyquist (a) and The phase angle and Bodeplots (b) representations.

Table 7. Electrochemical parameters extracted from the EIS curves in Figure 7.

c_{H_2S}	R_s	C		R_f	Q_{dl}		R_{ct}		
(ppm)	(Ω cm^2)	(Ω^{-1} cm^{-2} S^n)	n_f	(Ω cm^2)	(Ω^{-1} cm^{-2} S^n)	n_{dl}	(Ω cm^2)	R_L	L
5	5.161	1.837×10^{-5}	1	4.235	5.437×10^{-5}	0.803	1944	-	-
10	4.797	1.742×10^{-5}	-	4.701	4.778×10^{-5}	0.766	2660	541.7	185.9
20	7.091	1.489×10^{-5}	1	2.609	7.304×10^{-5}	0.791	2086	-	-
40	5.760	3.155×10^{-5}	1	3.112	1.181×10^{-4}	0.729	1479	-	-
80	4.158	7.293×10^{-5}	0.454	2.744	7.442×10^{-5}	0.912	1385	-	-
160	6.855	3.532×10^{-4}	0.803	115.9	2.533×10^{-4}	0.763	971.7	-	-
320	5.478	1.393×10^{-4}	0.877	241.6	3.295×10^{-4}	0.551	853.1	-	-

The reactions between iron and NH_4Cl, CO_2 and H_2S can be presented by the following equations:

$$Fe + 2NH_4^+ + 2Cl^- \rightarrow Fe^{2+} + 2NH_{3(l)} + H_{2(g)} + 2Cl^- \quad [1]$$

$$H_2S + Fe + H_2O \rightarrow FeS_{(s)} + H_{2(g)} + H_2O \quad [2]$$

$$Fe + CO_2 + H_2O \rightarrow FeCO_3 + H_2 \quad [3]$$

revealing that the corrosion products included FeS and $FeCO_3$. For 5 ppm H_2S, the amount of corrosion FeS product was small, resulting in poor protection of the carbon steel. In this case, the Cl^- ions had the smaller van der Waals radii [15] than other corrosive species (H^+, H_2S, CO_2, H_2O) [16, 17], which yielded a faster adsorption rate on the surface of carbon steel, thus accelerating the corrosion of carbon steel. At the H_2S concentration of 10 ppm, the CR value of carbon steel in the NH_4Cl-H_2S-CO_2 environment was minimum (0.7 mm/y) at 60°C. Therefore, this content of H_2S exerted a delaying effect on the corrosion rate, which was attributed to the formation of a thin FeS film on the steel surface that suppressed the anodic dissolution reaction. Besides, the presence of NH_4^+ ions increased the pH level of the solution, thus favoring the absorption of OH^- ions rather than Cl^- species on the steel surface and hence reinforcing protectiveness of the latter [18]. With increasing H_2S content from 10 to 320 ppm, the corrosive environment became more acid, thereby accelerating dissolution of the iron carbonate film [19] and augmenting the corrosion rate of carbon steel. The relationship between the corrosion rate and the H_2S concentration (10-320 ppm) can be expressed as follows:

$$Cr = -0.432e^{\frac{-c_{H_2S}}{34.59}} + 0.421 \quad [4]$$

and the corresponding plot is given in Fig. 8.

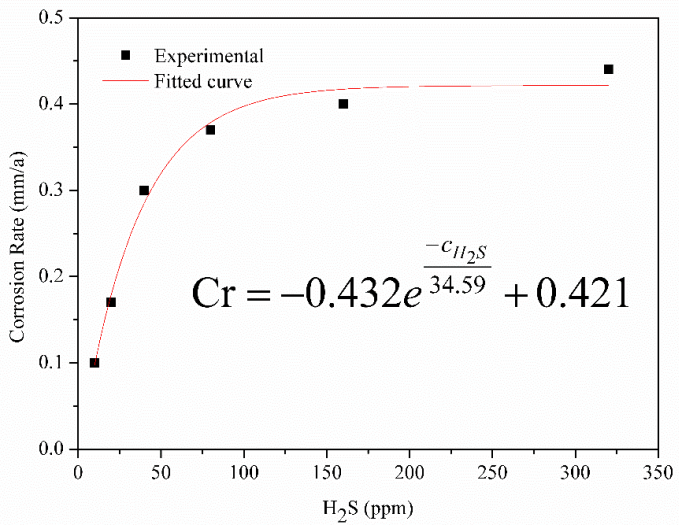

Figure 8. The CR values of carbon steel in NH_4Cl (0.5 mol %) solution with CO_2 (saturated) at different H_2S concentrations (10-320 ppm) at 60°C.

4. CONCLUSIONS

The corrosion behavior of carbon steel in the NH_4Cl-H_2S-CO_2 coexistence environment was studied. According to the results, the corrosion rate of carbon steel was 0.07 mm/y and the diameter of the capacitive loop was 2660 $\Omega \cdot cm^2$ in 0.5 mol% NH_4Cl solution with saturated CO_2 and the H_2S concentration of 10 ppm at 60 ℃. Under this condition, the corrosion rate was minimal. Moreover, the experimental data revealed that the presence of 10 ppm H_2S led to a reduction in the corrosion rate of the steel. At higher H_2S concentrations (10-320 ppm), the corrosion rate increased rapidly and the relationship between the corrosion rate and the H_2S concentration was established as well. In the NH_4Cl-CO_2-H_2S environment, the dominant cathodic reaction at a lower pH level (pH < 4) was the hydrogen reduction and that at a higher pH (pH > 4) was assigned to the carbonic acid reduction.

ACKNOWLEDGMENTS
This project was supported by the Liaoning Province Education Administration (LQ2020023) and the Liaoning Province Natural Science Foundation of china (2020-BS-169).

References

1. X.F. Liu, A.Q. Duan, J.X. Quan, H.Z. Jin and C. Wang, *Eng. Fail. Anal.,* 112(2020) 104529.
2. X.F. Liu, H.Y. Zhu, C.Y. Yu, H.Z. Jin, C. Wang and G.F. Ou, *Eng. Fail. Anal.,* 152(2021) 105448.
3. J. Hesketh, E.J.F. Dickinson, M.L. Martin, G. Hinds and A. Turnbull, *Corros. Sci.,* 182(2021) 109265.
4. D.Z. Zeng, B.J. Dong, F. Zeng, Z.M. Yu, W.G. Zeng, Y.J. Guo, Z.D. Peng and Y. Tao, *J. Nat. Gas. Sci. Eng.,* 86(2021) 103734.
5. G.A. Zhang, Y. Zeng, X.P. Guo, F. Jiang, D.Y. Shi and Z.Y. Chen, *Corros. Sci.,* 65 (2012) 37.
6. Z.Y. Liu, X.Z. Wang, R.K. Liu, C.W. Du and X.G. Li, *J. Mater. Eng. Perform.,* 23(2014) 1279.
7. M. Nimmervoll, A. Schmid, G. Mori, S. Honig and R. Haubner, *Corros. Sci.,* 181 (2021) 109241.
8. B.J. Dong, W. Liu, L. Cheng, J.D. Gong, Y.B. Wang, Y.C. Gao, S.X. Dong, Y.G. Zhao, Y.M. Fan, T.Y. Zhang and L.J. Chen, *Eng. Fail. Anal.,* 124(2021) 105364.
9. L.Y. Li, J. Yan, J. Xiao, L. Sun, H.Y. Fan and J. Wang, *Corros. Sci.,* 187 (2021) 109472.
10. G. Svenningsen, A. Palencsár and J. Kvarekvl, in NACE Corrosion 2009, Georgia (2009), p 09359..
11. H.B. Wang, Y. Li, G.X. Cheng, W. Wu and Y.H. Zhang, *J. Mater. Eng. Perform.,* 27(2018) 2492.
12. C.A. Shargay, J. Turner, B. Messer, W.C. Fort and D. Fan, NACE Corrosion 2001, Texas (2001), p 01543.
13. S. Wei and S. Nesic. NACE Corrosion 2007, Nashville (2007), p 07655.
14. Z.D. Cui, S.L. Wu, S.L. Zhu and X.J. Yang, *Appl. Surf. Sci.,* 252 (2006) 2368.
15. C. Zhang and J. Zhao, *Corros. Sci.,* 126(2017) 247.
16. C.D. Taylor, *Corrosion,* 68(2012) 591.
17. Y.G. Yan, X. Wang, Y. Zhang, P. Wang, X.H. Guo and J. Zhang, *Corros. Sci*., 73(2013) 123.
18. C.D. Taylor, *Int. J. Corros.,* (2012) 204640.
19. M.A. Pletnev, S.G. Morozov and V.P. Alekseev, *Prot. Met.,* 36(2000) 202.
20. M.B. Kermani and A. Morshed, *Corrosion,* 59 (2003) 659.
21. M. Singer, A. Camacho, B. Brown and S. Nešic, *Corrosion,* 67 (2011) 085003.
22. R.D. Kane and M.S. Cayard, NACE Corrosion 1998, California (1998), p 98274.
23. W. Huang, Sulfide stress cracking susceptibility of low alloy steels for casing application in sour environments. Diss. University of Alberta (Canada). 2012.

24. H.B. Wang, J.P. Yu and C.S. Lu, *Trans. Indian. Inst. Met.,* 74(2021) 2631.